JOURNAL LA MULTIAPP

VOL. 05, ISSUE 04 (453-464), 2024
DOI: 10.37899/journallamultiapp.v5i4.1432

Numerical Study of Cavitation Phenomenon in a Venturi Tube

Muhammad Nanda Fatur Rachman[1], Damora Rhakasywi[1], Fahrudin[1]

[1]*Mechanical Engineering Department, Faculty of Engineering, Universitas Pembangunan Nasional Veteran Jakarta, Indonesia*

**Corresponding Author: Muhammad Nanda Fatur Rachman*
Email: muhammad.nanda.fr@upnvj.ac.id

Article Info

Article history:
Received 4 July 2024
Received in revised form 27 July 2024
Accepted 28 August 2024

Keywords:
Numerical Studies
Cavitation Phenomenon
Venturi Tube
Throat Length Changes
Pressure Changes

Abstract

This research aims to understand and numerically analyze the cavitation phenomenon that occurs in Venturi tubes with variations in throat length and pressure changes. This research uses Ansys Fluent 2023 R2 numerical simulation with venturi tube geometries of 25 mm, 30 mm, and 35 mm and pressures of 300,000, 600,000, and 900,000 Pa. A multiphase flow model with water liquid and water vapor is applied to predict cavitation using a mixture model. RANS steady state conditions with the k-ε turbulence model are used to solve the continuity, momentum, energy and volume fraction equations. The Schnerr-Sauer cavitation model calculates the phase transition between water-liquid and water vapor. Geometry varies by reference journal with different converging and diverging angles, outlined in tables and figures. 2D simulations are carried out using a pressure based solver with specified boundary conditions, using the Presto! for pressure solutions, and upwind and Quick schemes for discretization. The results of this research show that 1) Length throat 25 mm has the most stable distribution compared to 30 and 35 mm geometries at a pressure of 600,000 Pa. 2) The cavitation phenomenon is influenced by changes in geometry where at 35 mm geometry greater cavitation occurs in the area near the wall inlet convergent. 3) At a pressure of 900,000 Pa, the cavitation area that forms becomes larger and becomes a critical point in this journal.

Introduction

Cavitation is a phase change process from liquid to vapor due to a decrease in pressure and occurs when there is a narrowing in the path through which the fluid flows. This process is widely used in several types of industries such as synthetic biodiesel production and water purification industries. One of the cavitation phenomena occurs in the venturi tube. A venturi tube is a tube used to measure the flow rate of a fluid, with one of its applications being in wastewater treatment processes. Generally, the venturi tube consists of three parts: converging, diverging, and throat (Ahad et al., 2022; Khan et al., 2022).

In certain cases, the use of a venturi tube aims to increase the efficiency of particle flow. The efficiency itself depends on the cavitation phenomenon occurring within the venturi tube and the interaction with turbulent flow. Therefore, the geometry of the venturi tube plays a crucial role in this phenomenon, such as the length of the throat, the diameter of the throat, and the convergent and divergent angles at the inlet or outlet. According to the journal Abbasi et al. (2020), the venturi tube was studied using simulation methods with the geometry design shown in Figure 1. The study concluded that the convergent and divergent angles affect the

ISSN: 2716-3865 (Print), 2721-1290 (Online)

characteristics of the cavitation flow that occurs. A larger convergent angle increases the cavitation stretch but consumes more power (Xie et al., 2021).

In the journal Zheng et al. (2022), the research focused on understanding the impact of the length of the convergent and divergent sections on cavitation characteristics under varying pressure conditions to provide new insights into the design and application of the venturi tube itself. The conclusion of this journal is that the cavitation characteristics in the throat area are not affected by changes in the length of the divergent section. However, the impact resulting from changes in the length of the divergent section depends on the pressure changes applied. On the other hand, the effect of changes in the convergent section is inversely related to the divergent section, where it influences the cavitation process. Meanwhile, in the journal Wilson et al. (2021), a study was conducted to determine the effect of geometry on microbubble cavitation in the venturi tube. The lower the angle of the diverging outlet, the better the cavitation efficiency.

According to the journal Park & Song (2022), simulations were conducted using the 2D-Axis-symmetric and 3D-CFD based models. With two types of viscosities from water-liquid or phase one 0.001 kg/m-s and 0.01 kg/m-s, and two types of Reynolds numbers. In the two-dimensional modeling, cavitation results were greater than in 3D compared to 3D (Simanto et al., 2022). Other studies with other two-dimensional models state that cavitation phenomena in the venturi tube often occur at the upper wall of the throat. By changing the pressure at the outlet and not doing so at the inlet, the distance of the cavitation phenomenon becomes longer, and the critical pressure ratio point is 1.192, below which nothing happens (Zhang et al., 2022).From the studies mentioned, it is clear that geometry and pressure changes at the inlet and outlet affect the cavitation phenomena occurring in the venturi tube. Therefore, based on the above formulation, this journal discusses cavitation phenomena concerning geometric changes and pressure changes at the inlet provided in the venturi tube using numerical methods.

Methods

Governing Equation, Turbulence, and Cavitation Model

The numerical simulation conducted to address the issues in this study uses computational methods with the software Ansys Fluent 2023 R2 (Ramos et al., 2023). In this journal, the geometries used are 25 mm, 30 mm, and 35 mm, where these values represent the throat length (L3), while the pressures applied are 300,000, 600,000, and 900,000 Pa. To predict the cavitation phenomena occurring in the venturi tube, the multiphase flow model available in Ansys setup mixture flow model for a single fluid was used. The initial fluid flow condition is water-liquid as phase-1 and water-vapor as phase-2 with the physical properties listed in Table 1.

Table 1. Physical properties used in the material setup

Material	ρ (kg/m^3)	μ (kg/m-s)
Water-liquid	998.16	0.001
Water-vapor	0.0173	9.727 x 10^{-6}

In this study, steady-state RANS (Reynolds-Averaged Navier Stokes) conditions are applied to solve the numerical problems. The κ-ε turbulent model is used because it is suitable for the 2D simulation of the venturi tube in this case. κ is turbulent kinetic energy, and ε is the turbulent dissipation rate. With the RANS approach to interpret the continuity transport equation governing mixture, momentum, energy, and phase change for the volume fraction equation are as follows:

$$\frac{\partial}{\partial t}(\rho m) + \nabla . (\rho_m \vec{v}_m) = 0$$

ISSN: 2716-3865 (Print), 2721-1290 (Online)

$$\frac{\partial}{\partial t}(\rho m) + \nabla.(\rho_m \vec{v}_m \vec{v}_m) = -\nabla P + \nabla.[(\mu_m + \mu_t)(\nabla \vec{v}_m + \nabla \vec{v}_m^T)]$$

Here, $\rho m, \mu_m$ and $\vec{v}_m$ are the density, viscosity, and velocity of the mixture-phase, respectively. The turbulent viscosity μ_t is calculated with the following equation:

$$\mu_t = \rho_m C_\mu \frac{k^2}{\varepsilon}$$

The transport equations for κ and ε can be written as follows:

$$\frac{\partial}{\partial_t}(\rho k) + \frac{\partial}{\partial x_i}(\rho k v_i) = \frac{\partial}{\partial x_j}\left[\left(\mu + \frac{\mu_t}{\sigma_k}\right)\frac{\partial k}{\partial x_j}\right] + G_k - \rho\varepsilon$$

$$\frac{\partial}{\partial t}(\rho\varepsilon) + \frac{\partial}{\partial x_i}(\rho\varepsilon v_i) = \frac{\partial}{\partial x_j}\left[\left(\mu + \frac{\mu_t}{\sigma_\varepsilon}\right)\frac{\partial \varepsilon}{\partial x_j}\right] + C_{1\varepsilon}\frac{\varepsilon}{k}(G_k + C_{3\varepsilon}) - C_{2\varepsilon}\rho\frac{\varepsilon^2}{k}$$

Where,

$$G_k = \mu_t S^2, \quad S = \sqrt{2S_{ij}S_{ij}}, \quad S_{ij} = \frac{1}{2}\left(\frac{\partial v_j}{\partial x_i} + \frac{\partial v_i}{\partial x_j}\right)$$

In the above equations, G_k is the production of kinetic energy due to velocity gradients, S is the modulus of the mean rate-of-strain tensor, and S_{ij} is the mean strain rate. The values of $C_{1\varepsilon}$ = 1.44, $C_{2\varepsilon}$ = 1.92, C_μ = 0.09, σ_k = 1, σ_ε= 1.3.

The Schnerr-Sauer cavitation model is applied to calculate the phase transition between the water-liquid and water-vapor phases. The vapor volume fraction is calculated with the transport equation for the vapor-phase as follows:

$$\frac{\partial}{\partial t}(\alpha_v \rho_v) + \nabla.(\alpha_v \rho_v \vec{v}_m) = R_e - R_c$$

Here, α_v is the volume fraction of the vapor phase, ρ_v is the density of the vapor, and ρ_l is the density of the liquid. The phase change due to cavitation is influenced by the mass transfer law. R_e and R_c are related to the evaporation and condensation of bubbles in the cavitating flow within the venturi tube. The equations used to describe the evaporation and condensation processes are as follows:

When $P_v \geq P_\infty$,

$$R_e = \frac{\rho_v \rho_l}{\rho_m}\alpha_v(1-\alpha_v)\frac{3}{R_b}\sqrt{\frac{2}{3}\frac{P_v - P_l}{\rho l}}$$

When $P_v \leq P_\infty$,

$$R_c = \frac{\rho_v \rho_l}{\rho_m}\alpha_v(1-\alpha_v)\frac{3}{R_b}\sqrt{\frac{2}{3}\frac{P_v - P_l}{\rho l}}$$

The volume fraction equation used to solve this problem is as follows:

$$\alpha_v = \frac{V_v}{V_m} = \frac{n_b \frac{4}{3}\pi R_b^3}{1 + n_b \frac{4}{3}\pi R_b^3}$$

The bubble radius can be solved with the equation:

ISSN: 2716-3865 (Print), 2721-1290 (Online)

$$R_b = (\frac{\alpha_v}{1-\alpha_v}\frac{3}{4\pi n_b})^{\frac{1}{3}}$$

Studies by Rodio (2011) and Chakraborty et al. (2024) assume a bubble number density of 10^{13}, which is optimal for validation. This journal uses the same value and modeling with the saturation vapor pressure of water P_v calculated at 2338 Pa at a temperature of 20ºC using the Antoine equation (Ansys Fluent Theory Guide, 2021):

$$LogP_v = A - \frac{B}{T+C}$$

The values of A, B, and C are 8.07131, 1730.63, and 233.426, respectively, which are substance specific constants. In this study, a large number of microscopic bubbles in the water phase is the onset of cavitation.

Geometry Model

This study varies the geometry based on the reference journal to understand the differences in phenomena and pressures that occur with changes in the converging and diverging angles of the venturi tube. The details of the geometry used are shown in Figure 2.1 and the geometric description in Table 2.

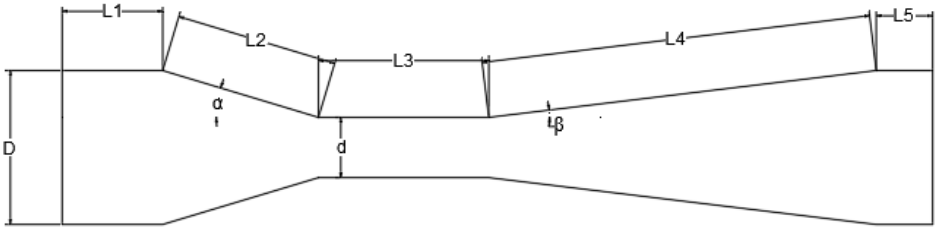

Figure 1. Venturi Tube Geometry

The geometrical representation of Venturi tube is used to analyze the effect of changes in the geometry of the tube on the velocity of the fluid and the formation of cavitation. The length and the angle of the converging section, the throat and the diverging section considerably influence the pressure and velocities across the diameter of the tube. The convergence angle (α) and divergence angle (β) are very important since it describes the fluid acceleration and deceleration which are fundamental in the occurrence of cavitation. This made it possible to foresee where and how cavitation might happen in order to regulate it in accordance with the particular industry the tube is to serve.

Table 2. Geometric Description Of Each Venturi Tube

Diameter (mm)	**12,7**
D (mm)	3,18
L1 (mm)	6
L2 (mm)	14
L3 (mm)	20
L4 (mm)	54
L5 (mm)	56
α (º)	19
β (º)	5

Table II below describes the specification of the Venturi tube used in the study in terms of the dimensions. The parameters enumerated above including the throat length (L3) and the angles α and β are directly linked to the objectives of the study in an effort to determine the trends of cavitation due to these geometrical changes. Among the throat length differences (25 mm, 30 mm, and 35 mm), the three tested lengths are important because they are the primary factor

ISSN: 2716-3865 (Print), 2721-1290 (Online)

under examination concerning cavitation with the expectation that differences in throat length will lead to differences in the pressure drop and flow interference and hence the degree of cavitation observed.

Solution Strategy

The simulation conducted is a 2D analysis of the venturi tube model with the boundary conditions used shown in Table 2.2. The numerical solution is solved using a pressure-based solver. The working fluid applied is water-liquid and water vapor. In the method section, the pressure solution applied is PRESTO! (PREssure STaggering Option). For turbulent kinetic energy and turbulent dissipation rates, second-order upwind discretization is used, and for momentum and vapor, second order upwind discretization and QUICK (Quadratic Upwind Interpolation for Convection Kinematics) are applied. The Coupled scheme method is utilized for Pressure-Velocity Coupling. This entire simulation is conducted under steady-state conditions.

Table 3. Boundary conditions

Name	Model/Scheme
Multiphase Flow	Mixture
Volume fraction parameter	Implicit Scheme
Viscous Model	RANS k- ε model
Cavitation Model	Schneer-Sauer
Pressure-Velocity Coupling	Coupled Scheme
Spatial Discretization-Gradient	Least Square Cell Based
Spatial Discretization-Pressure	PRESTO!
Spatial Discretization-Momentum	First Order Upwind
Spatial Discretization-Volume Fraction	QUICK
Spatial Discretization-Turbulence	Second Order Upwind

Pertaining to Table 3, matters regarding boundary conditions and numerical schemes used in the simulation are discussed in detail; thus, merely stressing on obtaining a logical and efficient way of simulating the cavitation inside the Venturi tube. With the employment of the multiphase flow model, and the combination with the cavitation model by Schnerr-Sauer, the changes of phase between the water liquid and the water vapor are well addressed. The RANS k-ε model is chosen due to satisfactory performance cost balance in simulating turbulent flow. Further, the presumed volume fraction scheme in common cases is the PRESTO! Combined with pressure discretization scheme, and for momentum and turbulence upwind and QUICK schemes respectively, they are all effective ways to respond to the unsteady flow dynamics and pressure gradientsIn addition to the choice of the discretization algorithm for pressure-velocity coupling, the setting is made more stable and accurate for the simulations around the regions of cavitating flow, so the overall setup proves sufficiently reliable for analysing the impact of the throat length and the pressure dynamics on the cavitating flow.

Results and Discussion

Grid Independence and Validation Model

Grid independence is a crucial step to determine the most effective mesh count for this research. The mesh counts applied in the venturi tube design include 40,000, 65,000, and 78,000 elements, all set up identically. These meshes were compared with previous experimental results. Among them, the 78,000-element mesh was found to be the most suitable for continuing the study on the effects of geometric changes on the venturi tube and the cavitation phenomena that occur (Wang et al., 2020).

ISSN: 2716-3865 (Print), 2721-1290 (Online)

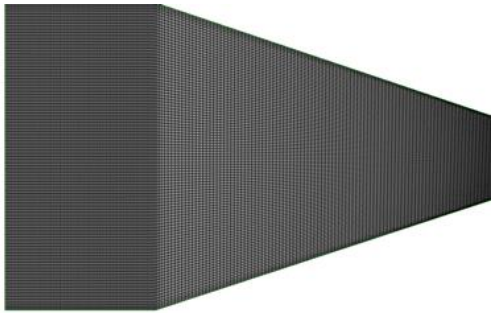

Figure 2. Mesh Structure Used in the Converging Section

In the numerical analysis for simulation, mesh structure plays important role so as to get the accurate and convergent solution. The analysis of the difference in mesh densities equals to 40000, 65000 and 78000 elements is presented in this work in order to determine the correlation between the difference in computational cost and the accuracy of the results received. The figure may show the increase of mesh density in the converging section of the Venturi tube where high velocity gradients tend to occur. This decision based on 78000 elements can be considered as the choice of the optimal mesh since the finer meshing improves the resolution of the flow characteristics, which is a critical factor for the proper prediction of the cavitation phenomena.

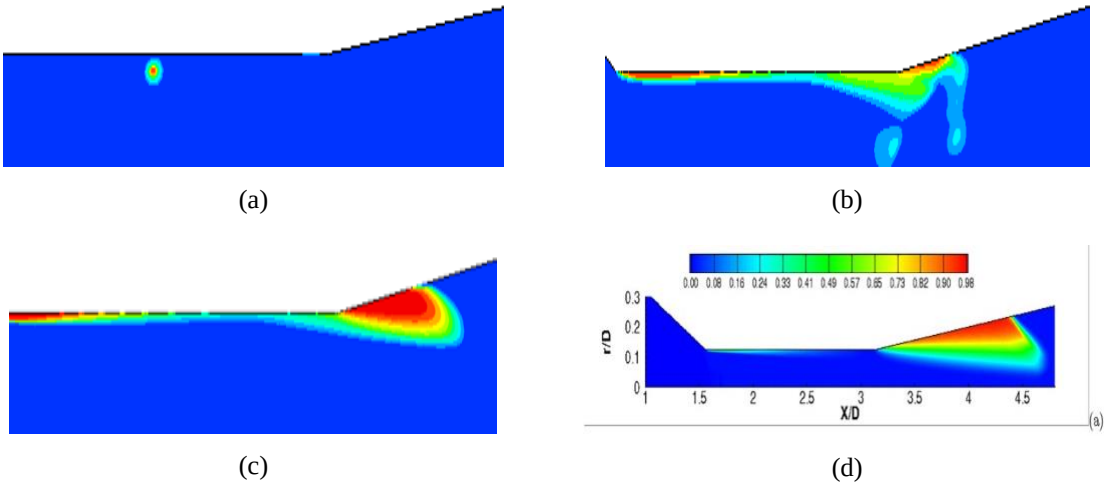

Figure 3. Volume Fraction Phase-2 in Each Element Mesh: (a) 40,000, (b) 65,000, and (c) 78,000. (d) Simulation Results (Lee et al., 2019)

Figure 3 is the comparison graph of the element mesh with the previous experiments Smith et al. , 2020 that they obtained an error rate with an average of 3. 28%. From this figure, it can be observed, the volume fraction of the vapor phase (a characteristic of cavitation), under the influence of varying mesh densities. As is clear from above, phase-2 volume fraction is a direct measure of cavitation intensity and location. The comparison with different mesh density also serves to check the validity of the present simulation as mesh density increases so that the phenomenon of cavitation is well predicted without requiring a huge amount of calculation. From this picture, one can observe that the 78000-element mesh has the least deviation from the final experimental values and thus, the mesh density used for the subsequent analysis was optimal.

Below figure shows the comparison of the simulation results in the using 78000-element mesh with the experimental data. The relatively large disparity means that the numerical model captures the Pressure Distribution and Cavitation Regions within the Venturi tube accurately; with an average error rate of only 3. 28.

ISSN: 2716-3865 (Print), 2721-1290 (Online)

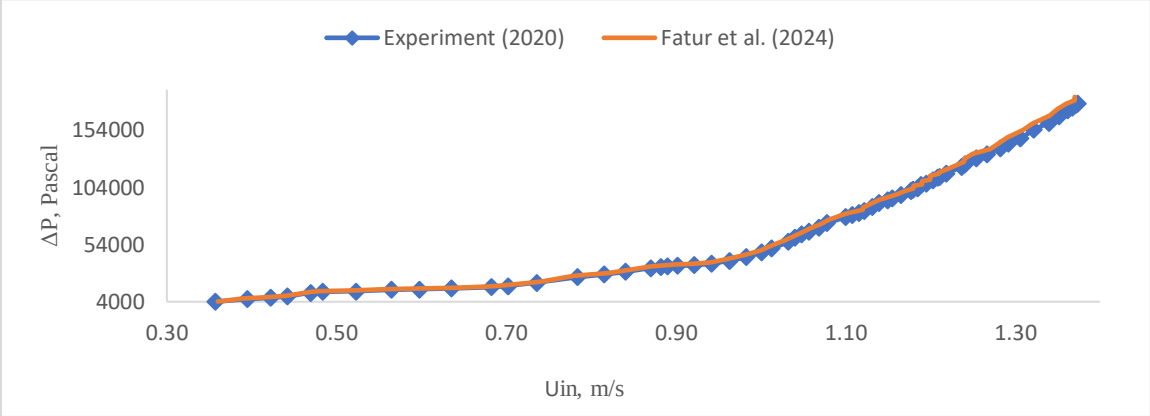

Figure 4. Comparison Graph of 78,000 Element Mesh with Experiment

This validation is important since it ensures that the selected numerical model and the mesh are valid for analysis of the impact of the geometrical and pressure changes in the Venturi tube cavitation.

Effects of Throat Length Changes on Venturi Tube Pressure

This journal investigates the changes in cavitation phenomena with three different throat lengths: 25 mm, 30 mm, and 35 mm. The shorter the throat length, the higher and slower the pressure distribution within the venturi tube (Huang et al., 2021). This is due to the fluid encountering the throat walls, preventing changes in the inlet velocity. As the throat geometry increases, the pressure distribution changes accordingly.

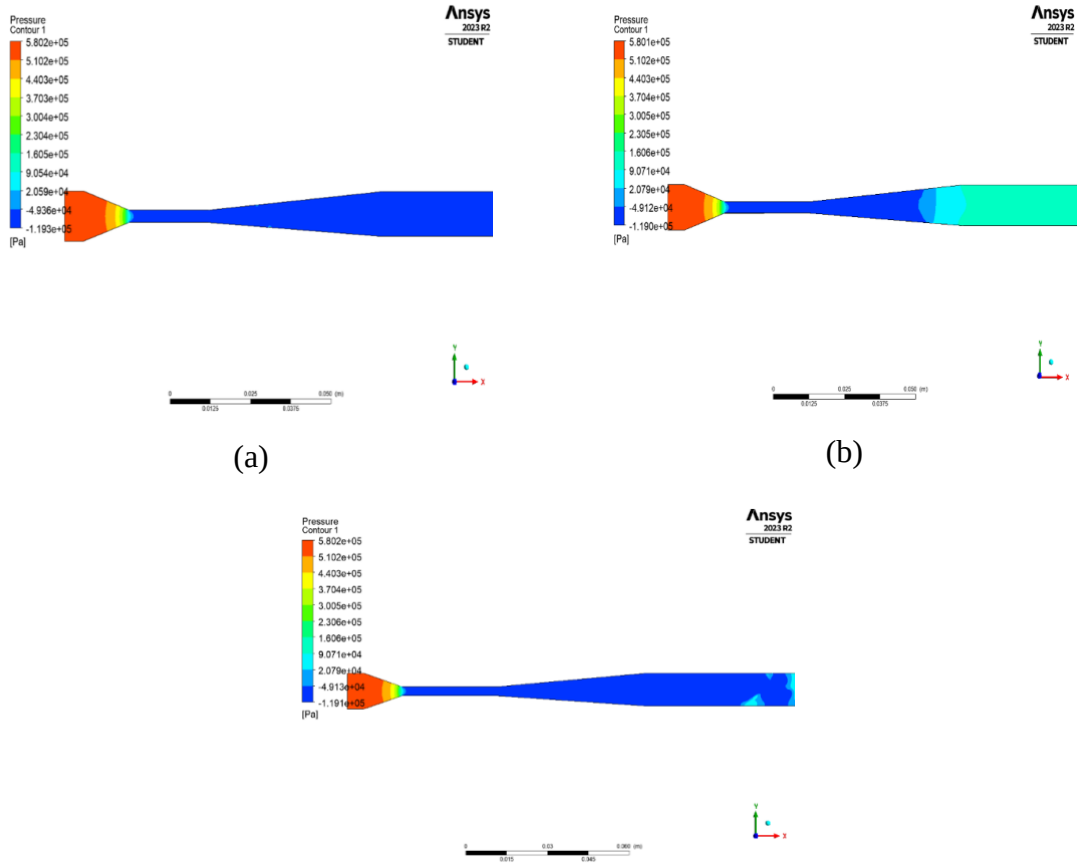

Figure 5. Pressure Distribution Contours in the Venturi Tube: (a) Geometry-1, (b) Geometry-2, and (c) Geometry-3 at 600,000 Pa

ISSN: 2716-3865 (Print), 2721-1290 (Online)

In the 25 mm throat length, shown in Figure 5, pressure distribution predominantly occurs near the outlet and decreases near the converging section before gradually increasing again (Liu & Li, 2023). This geometry results in more random pressure fluid flow. In contrast, the 30 mm and 35 mm geometries have more stable pressure distributions towards the outlet.

The pressure distribution contours given below depict the pressure distribution of the Venturi tube at 600000 Pa for different throat length The pressure distribution of the 25 mm throat length is comparatively random The 30 mm and 35 mm throat length has more or less regular pressure distribution. This stability is important in applications whereby an accurate controlling of the pressure is of great importance. This is evident in the random pressure distribution associated with the shorter throat length, which may imply more turbulence and possible instability of cavitation behavior thereby making the longer throat lengths more effective in delivering the required controlled cavitation.

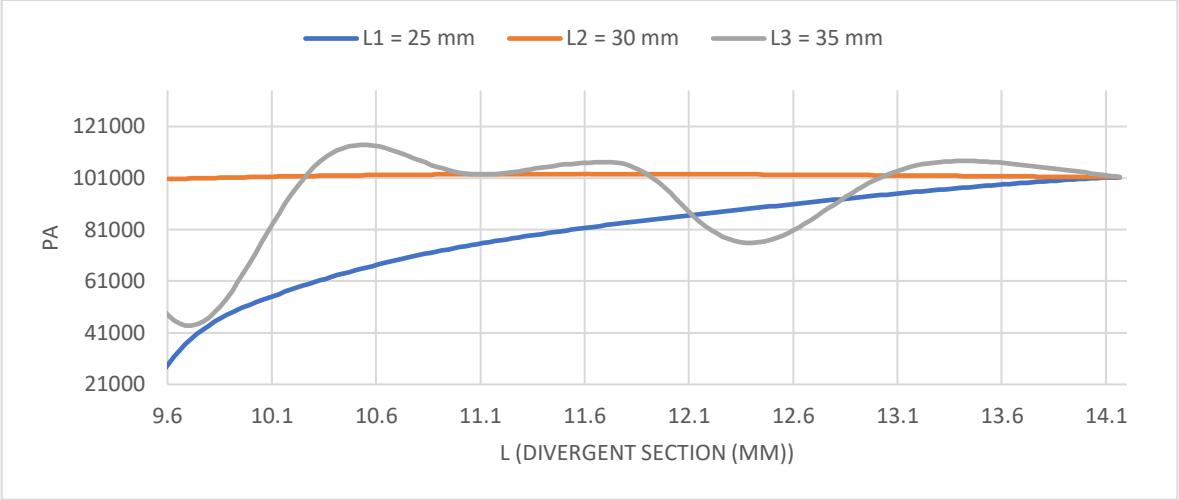

Figure 6. Static Pressure Graph for Each Throat Length Variation

The graph shown below describes the variation of static pressure in the Venturi tube with varying throat length. This means that 30 mm throat length offers the most stable pressure distribution especially in the region designed for divergence. This stability is important in order to avoid uncontrolled cavitation which leads to tube damage and reduction of efficiency. From the results, it can be safely concluded that there is an ideal throat length which will create a stable pressure distribution around this area and decrease the possibility of the occurrence of cavitation while at the same time will provide efficient flow conditions.

The changes in throat length (L3) for geometry-1 (25 mm), geometry-2 (30 mm), and geometry-3 (35 mm) at 600,000 Pa pressure affect the pressure distribution in the venturi tube as shown in Figures 5 and 6. The most stable distribution occurs at the 30 mm throat length in the divergent section. The shorter throat length in geometry-1 results in slower fluid velocity increases and slower distribution due to the direct relationship with velocity. Conversely, in geometry-3, the longer throat length causes unstable pressure distribution from the throat wall towards the divergent section.

Effects of Throat Length Changes on Cavitation Phenomena

Figure 7 shows different cavitation phenomena at the throat for geometry-1 (25 mm), geometry-2 (30 mm), and geometry-3 (35 mm). The different throat lengths lead to varying turbulence points. In geometry-1, cavitation predominantly occurs on the upper divergent wall and is shorter than in the other geometries. This phenomenon is influenced by the throat length, with more pronounced effects occurring.

ISSN: 2716-3865 (Print), 2721-1290 (Online)

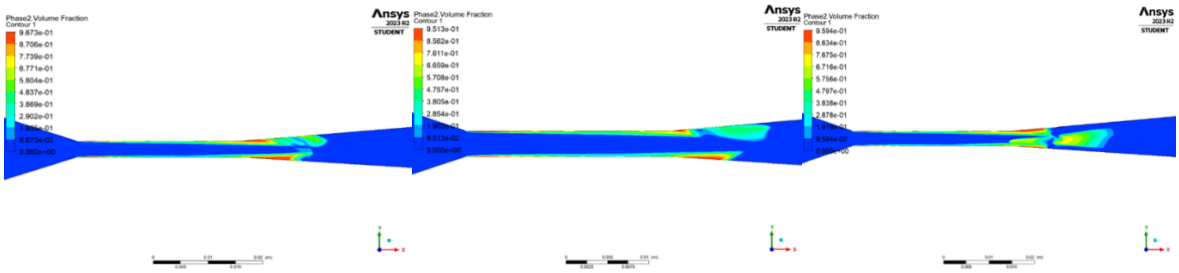

(a) (b) (c)

Figure 7. Cavitation Phenomena in Each Geometry: (a) Geometry-1, (b) Geometry-2, and (c) Geometry-3 at 300,000 Pa

In this figure the cavitation regions as a function of the throat length are indicated. Compared with the general characteristics of the throat section, it is seen that the cavitation is most severe near the upper divergent wall in the 25mm throat length profile, which proves that shorter throat lengths are more susceptible to cavitation, likely due to increased turbulence and pressure losses. This insight is very useful for applications where minimizing and managing cavitation is of high importance in an attempt to eliminate the effects that are usually detrimental to the device in question. The figure shows that short throat length will actually give high flow rates but the trade off is that it leads to more cavitation which is undesirable in long term applications.

Effects of Pressure Changes on Cavitation Phenomena in the Venturi Tube

Pressure changes in geometry-1 at pressures of 300,000, 600,000, and 900,000 Pa are examined. As shown in Figure 8, the cavitation area increases near the converging inlet wall. The cavitation area in the venturi tube is significantly influenced by the inlet pressure. Higher pressures result in larger cavitation areas when the fluid passes through the throat. At 600,000 Pa, the cavitation area reaches a critical point, producing significant cavitation.

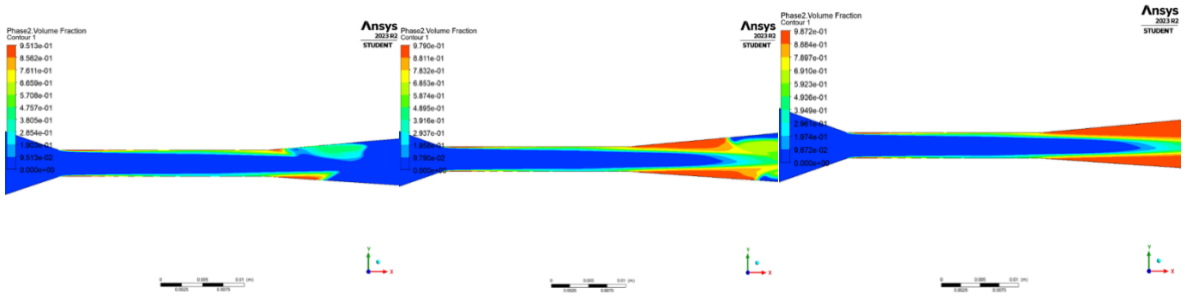

(a) (b) (c)

Figure 8. Cavitation Phenomena at 25 mm Throat Length: (a) 300,000 Pa, (b) 600,000 Pa, and (c) 900,000 Pa

The figure reveals how cavitation regions are developed with inlet pressure at an increasing range of 300000 Pa to 900000 Pa for 25 mm of throat length. Cavitation area is greatly increased as pressure is increased further helps in understanding the importance of pressure in cavitation formation. This information is useful for establishing systems that have to work at different pressures since this table shows that, maximum pressures which, enhance flow rates at the same time enhance the occurrence of cavitation which is a serious issue as it may cause damage or make the system to be inefficient.

Perhaps one of the most interesting findings of this study is the impact of throat length to cavitation, especially in realising that shorter lengths such as the 25 mm configuration have a tendency to intensify turbulent flow conditions. This observation is consistent with prior work that highlighted the destabilizing influence of short throat lengths and demonstrates that this

ISSN: 2716-3865 (Print), 2721-1290 (Online)

turbulence results in highly localized, stochastic cavitation near the upper divergent wall (Simpson & Rande, 2019). The implications for industrial applications are significant: though reduced throat lengths can be preferred for specific flow conditions, they may cause dangerous throat cavitation, resulting in material erosion and system performance decrement This finding implies a new perspective on design approaches in any systems where cavitation control is critical, indicating that the contending issues of flow rate and cavitation require more differentiation (Sloteman et al., 2013).

The study also poses threat to the conventional belief about uniformity of pressure distribution stability. The identification of the 30 mm throat length as offering the maximum pressure distribution stability particularly in the divergent part of the diffuser changes perspectives from simply avoiding cavitation to optimizing the flow regime to offer the best balance between stability and efficiency. This knowledge is even more pivotal in areas like hydraulic machinery for instance, since the structure of the pressure often has a massive influence on the kind of stability required in equipment (Zemanová & Rudolf, 2020).

The study is useful for coming up with a better understanding of how the throat length can be fine-tuned for better performance while avoiding the risks of cavitation by suggesting that a moderate throat length provides adequate stability.Furthermore, an increased inlet pressure has been identified in the study at 900000 Pa to have a tremendous effect of causing a larger cavitation area. It is not simply a verification of an already-known theory which is workable, but an expansion that extensively points out at the curve of pressure and cavitation intensity. The found threshold pressure beyond which cavitation is uncontrollable, as obtained in this research, serves as significant guideline for the design and management of the fluid systems. This implies that there is need to be more careful in managing inlet pressure because there is tendency that change in cavitation can be more drastic once the operational limits are crossed (Zheng et al., 2022). This is more applicable to industries that use high pressure systems for example in fuel injection or in water purification where effects of uncontrolled cavitation may prove disastrous.

The authors have done well in employing and applying Schnerr-Sauer cavitation model, Reynolds-Averaged Navier–Stokes (RANS) k- ε turbulence model and in ensuring methodological rigorous for this studyChoosing a 78000-element mesh also adds to the credibility of the results so that none of the complex interactions within the Venturi tube are missed in the simulation. On the one hand, the fact that steady-state conditions were chosen for simulation adds value, but on the other hand, it is a limitation (Román-Ancheyta et al., 2021). Consequently, cavitation is most explicitly a process in time and it might be even more revealing to analyze the process with time dependent simulations. This would most probably provide more information on the interaction between cavitation bubbles and the material and design of the components involved, on how the bubbles develop and collapses thus giving the deeper understanding to control cavitation in any practical application (Sarraf et al., 2022; Kadivar et al., 2024).

One of the special features of this work also lies in the fact that it can make a significant contribution to the development of the further theory of fluid dynamics and new approaches to the study of cavitation processes (Omelyanyuk et al., 2022). In addition to replicating the results of prior research, by a applying the gathered information in a new setting, the study contributes to expanding the state of knowledge. The findings concerning the design implications of Venturi tubes are especially worth highlighting since the work offers practical recommendations regarding the correlation between geometry and operation conditions to minimize the threats of cavitation. It is a significant contribution to the academic body of knowledge as this work presents theoretical developments as well as strategies that can be implemented in engineering practice.

ISSN: 2716-3865 (Print), 2721-1290 (Online)

Conclusion

Today With the importance of internet for everybody whether in private life or in practical live, we can imagine the world with out of internet specially with the smart application that presented to us, all the objectives around our environment can be connected to internet with a large network containing different sensors with standard protocol for IoT, and it provides the chance for people to control things over distance Without the need to be in a specific place to deal with a specific device, hence the IoT system that is used in this work is successfully using raspberry pi as an IoT device and HTTP post request for transferring the captured image file and server for receiving and store image. The future work will be about processing the image that stored in the server using training system and robost algorithm for processing using also hardware platform

ORCID

Damora Rhakasywi https://orcid.org/0000-0001-8844-3508

References

Ahad, J., Farooq, A., Siddique, W., Ahmed, A., Ahmad, M., Waheed, K., ... & Irfan, N. (2022). Influence of variation in converging section and orifice plane on the performance of venturi scrubber by using CFD. *Progress in Nuclear Energy*, *151*, 104323. https://doi.org/10.1016/j.pnucene.2022.104323

Khan, Z. A., Jain, N., & Anbu Kumar, S. (2022). Optimization of convergent angle of the Venturi meter for best coefficient of discharge. *Water Supply*, *22*(12), 9023-9040. https://doi.org/10.2166/ws.2022.381

Abbasi, E., Saadat, S., Jashni, A. K., & Shafaei, M. H. (2020). A novel method for optimization of slit Venturi dimensions through CFD simulation and RSM design. *Ultrasonics sonochemistry*, *67*, 105088. https://doi.org/10.1016/j.ultsonch.2020.105088

Xie, C., Liu, J., Jiang, J. W., & Huang, W. X. (2021). Numerical study on wetted and cavitating tip-vortical flows around an elliptical hydrofoil: Interplay of cavitation, vortices, and turbulence. *Physics of Fluids*, *33*(9). https://doi.org/10.1063/5.0064717

Wilson, D. A., Pun, K., Ganesan, P. B., & Hamad, F. (2021). Geometrical optimization of a venturi-type microbubble generator using CFD simulation and experimental measurements. *Designs*, *5*(1), 4. https://doi.org/10.3390/designs5010004

Park, Y., & Song, T. (2022, March). Plasma arc simulation of high voltage circuit breaker with a hybrid 2D/3D model. In *2022 6th International Conference on Electric Power Equipment-Switching Technology (ICEPE-ST)* (pp. 190-193). IEEE. https://doi.org/10.1109/ICEPE-ST51904.2022.9757101

Simanto, R. I. A., Hong, J. W., Kim, K. S., Ahn, B. K., & Shin, S. (2022). Experimental investigation on cavitation and induced noise of two-dimensional hydrofoils with leading-edge protuberances. *Physics of Fluids*, *34*(12). https://doi.org/10.1063/5.0127170

Zhang, J., Zhao, W., Liu, H., & Xi, G. (2022). Numerical study of surfactant effects on the rise of a single bubble and two coaxial bubbles. *International Communications in Heat and Mass Transfer*, *137*, 106284. https://doi.org/10.1016/j.icheatmasstransfer.2022.106284

Ramos, M. C., Costa, A. L., Silva, V. V. A., Lima, C. P. B., & Veloso, M. A. F. (2023). Numerical simulation and validation of laminar flow through a 2D pipe using computational fluid dynamics. *Brazilian Journal of Development*, *9*(10), 28793-28807. https://doi.org/10.34117/bjdv9n10-084

ISSN: 2716-3865 (Print), 2721-1290 (Online)

Rodio, M. G. (2011). *Numerical and experimental investigation of water and cryogenic cavitating flows* (Doctoral dissertation, Università degli studi di Lecce).

Chakraborty, B., Gallo, M., Marengo, M., De Coninck, J., Casciola, C. M., Miche, N., & Georgoulas, A. (2024). Multi-scale modelling of boiling heat transfer: Exploring the applicability of an enhanced volume of fluid method in sub-micron scales. *International Journal of Thermofluids*, *22*, 100683. https://doi.org/10.1016/j.ijft.2024.100683

Wang, L., Ji, B., Cheng, H., Wang, J., & Long, X. (2020). One-dimensional/three-dimensional analysis of transient cavitating flow in a venturi tube with special emphasis on cavitation excited pressure fluctuation prediction. *Science China Technological Sciences*, *63*(2), 223-233. https://doi.org/10.1007/s11431-019-9556-6

Huang, J., Sun, L., Mo, Z., Feng, Y., Bao, J., & Tang, J. (2021). Experimental investigation on the effect of throat size on bubble transportation and breakup in small Venturi channels. *International Journal of Multiphase Flow*, *142*, 103737. https://doi.org/10.1016/j.ijmultiphaseflow.2021.103737

Liu, Y., & Li, B. (2023). Numerical Investigation of the Cavitation Characteristics in Venturi Tubes: The Role of Converging and Diverging Sections. *Applied Sciences*, *13*(13), 7476. https://doi.org/10.3390/app13137476

Simpson, A., & Ranade, V. V. (2019). 110th Anniversary: comparison of cavitation devices based on linear and swirling flows: hydrodynamic characteristics. *Industrial & Engineering Chemistry Research*, *58*(31), 14488-14509. https://doi.org/10.1021/acs.iecr.9b02757

Sloteman, D. P., Redding, J., & Cooper, P. (2013, July). Evaluation and Analysis of an Early Inducer Design and Its Approach to Backflow Control. In *Fluids Engineering Division Summer Meeting* (Vol. 55553, p. V01BT10A018). American Society of Mechanical Engineers. https://doi.org/10.1115/FEDSM2013-16303

Zemanová, L., & Rudolf, P. (2020). Flow inside the sidewall gaps of hydraulic machines: a review. *Energies*, *13*(24), 6617. https://doi.org/10.3390/en13246617

Zheng, H., Zheng, Y., & Zhu, J. (2022). Recent developments in hydrodynamic cavitation reactors: Cavitation mechanism, reactor design, and applications. *Engineering*, *19*, 180-198. https://doi.org/10.1016/j.eng.2022.04.027

Sarraf, S. S., Talabazar, F. R., Namli, I., Maleki, M., Aghdam, A. S., Gharib, G., ... & Koşar, A. (2022). Fundamentals, biomedical applications and future potential of micro-scale cavitation-a review. *Lab on a Chip*, *22*(12), 2237-2258. DOI https://doi.org/10.1039/D2LC00169A

Kadivar, E., Rezaee, S., Löschner, U., & el Moctar, O. (2024). Effects of Materials and Riblets on Erosion Mitigation Induced by Multiple Collapses of Cavitation Bubbles. *Applied Sciences*, *14*(15), 6452. https://doi.org/10.3390/app14156452

Román-Ancheyta, R., Kolář, M., Guarnieri, G., & Filip, R. (2021). Enhanced steady-state coherence via repeated system-bath interactions. *Physical Review A*, *104*(6), 062209. https://doi.org/10.1103/PhysRevA.104.062209

Omelyanyuk, M., Ukolov, A., Pakhlyan, I., Bukharin, N., & El Hassan, M. (2022). Experimental and numerical study of cavitation number limitations for hydrodynamic cavitation inception prediction. *Fluids*, *7*(6), 198. https://doi.org/10.3390/fluids7060198

ISSN: 2716-3865 (Print), 2721-1290 (Online)